Microfluidic-Assisted Growth of Perovskite Single Crystals for Photodetectors

Ilenia Viola,* Fabio Matteocci, Luisa De Marco,* Leonardo Lo Presti, Silvia Rizzato, Simona Sennato, Alessandra Zizzari, Valentina Arima, Antonio De Santis, Chiara Rovelli, Silvio Morganti, Matthias Auf der Maur, and Marianna Testa*

The organometal halide perovskites (OMHP) are promising candidates for fast, sensitive, and large area photodetectors. In the last decade, several techniques have been developed with complementary advantages. Film devices are thin and can be scaled to large area, but have a large number of grain-boundaries related defects. Single bulk crystals instead have higher purity, but are thicker and can not be easily produced on large areas. In this work, a microfluidics-assisted technique to realize a controlled growth of OMHP single crystals, in the form of microwires, directly on a conductive patterned substrates, is presented. This technique enables the realization of vertical devices with a pixelated sensor layer. The resulting devices present gain, a responsivity up to 200 AW^{-1} and a fast rise time down to 35 µs. This is the first demonstration of a OMHP vertical device realized on a patterned substrate using microfluidics-assisted techniques.

1. Introduction

During the last decade, organometal halide perovskites (OMHP) have proven to be a promising and highly performing material for detection of both visible photons[1,2] and ionizing radiation,[3] beside their large success in photovoltaic devices.

OMHP based detector prototypes have been produced both based on thin film technology and on single crystal (SC) growth, using low-cost solution processes at low temperatures and under ambient conditions. Due to their intrinsic polycrystalline nature, OMHP films suffer from lower material quality compared to SCs due to grain boundaries and grain defects. Moreover, standard deposition techniques like spin or blade coating are typically limited to film thicknesses up to 1 µm, limiting their application to absorption in the visible spectrum. On the other hand, the fabrication processes used for single crystals based on seeding techniques are not directly suited for large area devices and cannot easily be combined with planar device technology.

Attempts to fabricate pixelated devices using micro-sized SCs, microplates and microwires are steadily growing. Both lateral and vertical devices, where the contacts are deposited, respectively, on the same or the opposite faces of the perovskite crystal have been documented. A comprehensive review on microstructured perovskite functional devices in opto-electronics has been

I. Viola
NANOTEC-CNR, Institute of Nanotechnology, Soft and Living Matter
Laboratory, c/o Physics Dept.
Sapienza Università di Roma
Piazzale A. Moro 2, I-00185 Rome, Italy
E-mail: ilenia.viola@nanotec.cnr.it

F. Matteocci, M. Auf der Maur
Department of Electronic Engineering
University of Rome Tor Vergata
Via Politecnico 1, 00133 Rome, Italy

L. De Marco, A. Zizzari, V. Arima
NANOTEC-CNR, Institute of Nanotechnology, c/o Campus Ecotekne
University of Salento
Via Monteroni, I-73100 Lecce, Italy
E-mail: luisa.demarco@nanotec.cnr.it

L. Lo Presti, S. Rizzato
Department of Chemistry
Università degli Studi di Milano
Via Golgi 19, 20133 Milano, Italy
E-mail: leonardo.lopresti@unimi.it

S. Sennato
ISC-CNR, Institute for Complex Systems, c/o Physics Dept
Sapienza Università di Roma
Piazzale Aldo Moro 2, I-00185 Rome, Italy

A. De Santis, M. Testa
INFN Laboratori Nazionali di Frascati
via E. Fermi 54, 00044 Frascati (RM), Italy
E-mail: marianna.testa@lnf.infn.it

C. Rovelli, S. Morganti
INFN Sez. di Roma, c/o Department of Physics
Sapienza Università di Roma
P.le Aldo Moro 2, 00185 Rome, Italy

published recently.[4] Generally, fewer studies are available in literature documenting vertical devices using micro-sized SCs, probably due to the larger difficulties in making the electrical contacts. However, vertical devices typically have a smaller distance between the contacts, a more uniform electric field and can be more easily integrated with commercial electronics. Due to the larger distance between the contacts, micro-sized lateral devices tend to have slower rise and decay times.

The first successful patterned growth by controlled nucleation of regular arrays of perovskite microplate SCs is reported from Wang et al.[5] The authors realized a lateral device with planar contacts on the same face of the SCs of 10 µm size. Inkjet-printed lateral photodetector arrays based on $CH_3NH_3PbI_3$ microwires with a width of 3 µm have been reported by Liu et al.,[6] showing a decay time of $\tau_d = 10$ ms and responsivity of $R = 1.2$ AW^{-1}. Chen et al.[7] presented a long-term stable lateral photodetector based on smaller microwires with 1–2 µm width fabricated by a dip-coating method, with rise time of 50 ms and responsivity up to 13.8 AW^{-1}. Surface passivated randomly-distributed microwires, obtained by a room-temperature wet-chemical synthesis in ref. [8] are used to fabricate a lateral photodetector with $R = 1.27$ AW^{-1}.

More recently, an array of cesium lead bromide perovskite ($CsPbBr_3$) microplates, obtained by vapor-phase growth with controllable size and location, have been fabricated by Gu et al.[9] and used to realize a lateral photodetector with a high responsivity up to 480 AW^{-1}. A vertical device instead was reported by Li et al.,[10] using an array of $CH_3NH_3PbBr_3$ ($MAPbBr_3$) microplates, growth by self-assembly on a pre-lithographed substrate, with thickness of 400–800 nm and lateral dimensions in the range from about 10–15 µm, exhibiting a low responsivity of 0.38 AW^{-1}. Furthermore, Wang et al.[11] reported a general method to fabricate large area arrays of SCs of size between 20 and 70 µm with space confined growth to produce a lateral UV photodetectors. A lateral device based on an array of $CsPbBr_3$ perovskite microwires embedded in silicon microchannels has been fabricated through a micropump fluidic strategy, as described in Xin et al.,[12] reaching $R = 0.96$ AW^{-1}. Significant long-term stability of lateral photodetectors based on microwire-arrays of $MAPbBr_3$ single crystals, fabricated by an edge-adsorption technique, and showing $R = 20$ AW^{-1} and a rise time $\tau_r = 1.6$ ms, have been reported by the group of Li.[13] An array of $CsPbBr_3$ microwires has been produced using a template-assisted method by Ren et al.,[14] showing a R up to 118 AW^{-1} and $\tau_r = 38$ ms. Deng et al.[15] reported a lateral device with $R = 13.5$ AW^{-1} and $\tau_r = 80$ µs, realized through arrays of aligned perovskite micro-wires from a blade coating technique.

Later, again Deng et al.[16] fabricated a vertical device based on an array of microchannels obtained through a microchannel-confined crystallization strategy with high $R = 2400$ AW^{-1} but a slow $\tau_r = 0.6$ s. In 2022, Li[17] presented $MAPbBr_3$ microwire crystal arrays on curved substrates, using a temperature gradient-assisted in situ nanoimprinting, and resulting in a curved-surface lateral photodetector with $R = 414$ AW^{-1}, $\tau_r = 3.2$ ms, characterized by crystals' height and width up to 422 nm and 2 µm, respectively.

Generally, the realization of high performance vertical opto-electronic devices based on perovskite single crystals still requires to overcome several difficulties. In particular, there is a need to grow crystals in precise positions of the device and with an accurate size control. Also, the fabrication of efficient vertical devices requires the growth of SCs with high aspect ratio, that is, with a large ratio between the lateral dimension and the thickness. A high aspect ratio allows to satisfy at the same time the request of efficient and fast charge collection realizable through a thin crystal, and the request of a sufficiently large area to easily integrate the electrical contacts in the final device.

To date, no direct growth method has demonstrated effective and simultaneous control of both the 3D structure of a perovskite SC (lateral dimensions, thickness, and therefore its aspect ratio) and its precise location on a patterned substrate.[10,16–19]
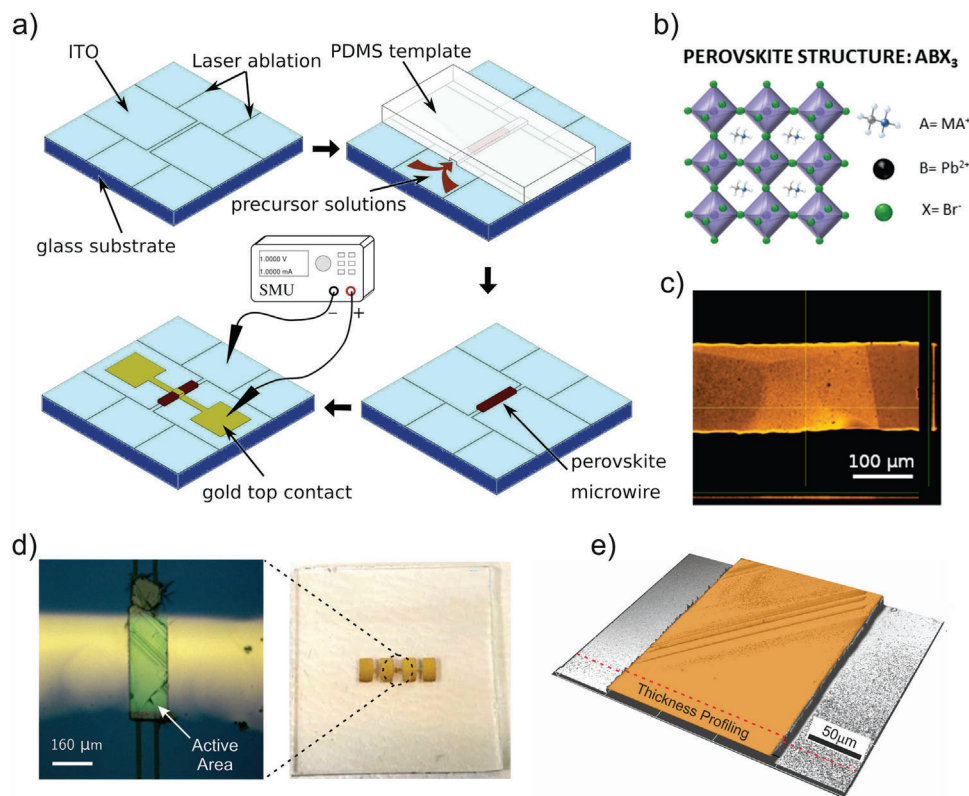
In this work, we show, for the first time, the realization of a vertical device based on perovskite SCs in the form of microwires, made through a simple and single-step microfluidic-assisted growth, directly on a conductive patterned ITO substrate. The used technique allows a high level of control over the SCs' growth position and their size. The fabrication approach also guarantees the possibility of growing SCs on several types of device interfaces. These SCs are easy-to-produce in a conventional laboratory environment, even in the presence of significant substrate steps, for example between insulating and conductive lines. All in all, the proposed approach allows the growth of perovskite crystals with desired geometric features directly on the interface of a functional optoelectronic device, thus enabling the realization of vertical photosensors or 2D large area arrays of photosensors, where the positive and negative contacts are on opposite faces of the crystals.

Such possibility to grow perovskite single crystals directly on patterned substrates with precise control on position, dimensions, and aspect ratios further opens up the road toward the integration of perovskite devices with silicon-based technology.

2. Results and Discussion
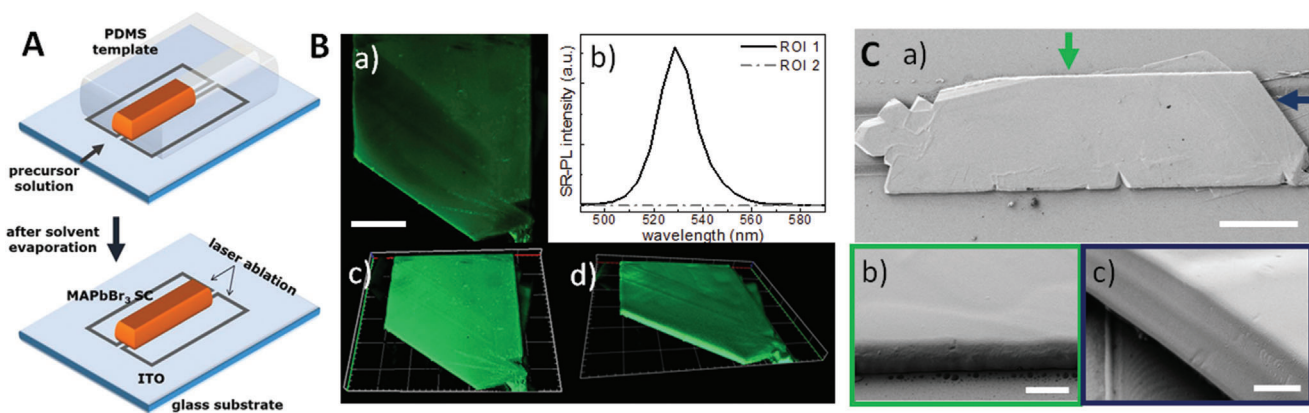
2.1. Device Fabrication

The fabrication of high quality perovskite SC microwires, with precise dimensions and structural characteristics, has been carried out using a microfluidic-assisted technique by exploiting a network of polymeric microchannels, schematically sketched in **Figure 1**a. The network of microchannels is usually realized with polymeric materials by soft-lithography. Here, we use polydimethylsiloxane (PDMS) as molding polymer because of its well-known high conformability, chemical inertness, optical transparency, and ease of functionalization. PDMS also allows to reproduce patterns with micrometer resolution and over large areas.[20] The PDMS template with a microchannel pattern is put into conformal contact with a patterned indium tin oxide (ITO)/glass substrate, where suitable conductive lines connected to pads have been defined via laser ablation. In this paper, a 150 µm wide microchannel is aligned to a 70 µm wide ITO stripe. The latter is used as bottom contact in the final detector device. The microchannels, thus obtained, are soaked with the precursor solution of $MAPbBr_3$ in dimethylformamide (DMF; Figure 1b).[21,22] Once the protocol for the fluid displacement has been optimized, after the precursor evaporation, SCs of the desired size and of high quality are obtained (Figure 1c), directly on patterned and conductive substrates for application within the devices (Figure 1d, right).

2300023 (2 of 9)

**ADVANCED
SCIENCE NEWS**

www.advancedsciencenews.com

**ADVANCED
MATERIALS
TECHNOLOGIES**

www.advmattechnol.de

Figure 1. a) Microfluidic-assisted growth of 3D perovskite microwire single crystals, aligned with the conductive lines on a laser-patterned ITO/glass substrate (not to scale). Perovskite precursor solution fills the polymeric microchannel and crystallizes into a SC microwire. After removal of the PDMS template, a gold top contact is evaporated, defining thus a vertical SC device. b) Crystal structure of MAPbBr$_3$ perovskite. c) Confocal z-stack image of the obtained SC shows the high quality growth on a conductive substrate. d) Picture of a working photo-detector realized on the micro-wire SC. The active region of the device is highlighted in the 10X optical image, where the laser ablation tracks are also visible. e) Confocal 3D imaging of the device used to measure the thickness profile of the microwires.

This result is guaranteed by a microfluidic-assisted deposition technique that allows finely modulate the dynamics of the liquid perovskite precursor within a microchannel network and, therefore, define position, shape, and dimensions of the micro-crystals directly obtained on different substrates. By modulating the internal pressure, temperature, wettability, and functionalization at the microchannels' interface, it is possible to regulate the distribution of the precursor solution confined within PDMS microchannels and thus the quality of SCs.[23,24] This allows to obtain functional 3D perovskite-SCs, with controlled features, tailored height, and lateral dimensions, and lengths in the millimeter range. As shown in Figure 1, the microwires are obtained by controlling the intermediate state (i.e., the precursor solution), during the nucleation and crystallization steps. This approach enables the fabrication of SCs with precise shape characteristics and on several types of substrates. The technique is independent of substrate roughness and the presence of steps at the interface of conductive substrates. Microfluidics also ensures high reproducibility in the structures and uniformity of the SCs obtained, by controlling the structural properties of soft PDMS template used for spatial confinement and the energetic parameters of liquid precursor displacement, confined within microchannels. PDMS templates with different microchannel sizes (widths in the range of 15–150 μm, and heights between 500 nm and

10 μm) were used in order to optimize the parameters involved in the crystallization process. In order to obtain the right structural alignment and high quality crystallinity, experiments were carried out by modulating: i) the molarity of perovskites precursor solution (from 0.3 to 1.4 M) in different organic solvents; ii) the growth temperature (in the range from 2 to 24 °C); iii) the geometric confinement in the range of 15–150 μm for the width and between 500 nm up to 10 μm for the height; iv) the energetic properties at the channel interface by using different type of wettability and functionalization; v) the speed of precursor displacement within microchannels; and vi) the substrate interface (glass, glass/ITO). The extreme flexibility of the fabrication technique and the possibility of acting on the different parameters of the fluidic process allow the precise optimization of the technique based on the type of SC required by a specific device. As shown in Figure 1 after the removal of the PDMS template, a nominally 140 μm wide gold top contact line is evaporated, oriented orthogonally to the perovskite microwire. Larger gold pads have been defined for easier contacting. The evaporation mask has been produced using 3D-printing, while the alignment with the perovskite micro-wire was performed manually under a confocal optical microscope. The active area of the device is defined as the overlapped area between the microwire and gold electrode. Since the 3D-printed mask allowed only limited control over the

**ADVANCED
SCIENCE NEWS**

www.advancedsciencenews.com

**ADVANCED
MATERIALS
TECHNOLOGIES**

www.advmattechnol.de

Figure 2. A) Sketch of single crystal growth process by microfluidic-assisted technique on patterned ITO substrate. B) Confocal characterization of a MAPbBr3 SC with a height of 6 µm: 2D confocal image obtained with a 405 nm-laser excitation and collecting the spectrum over the emission range (a); SR-PL of both an area of the crystal (ROI1) and an external part on the substrate (ROI2) (b); 3D z-stack reconstruction of the same SC obtained by the confocal acquisition over the crystal's thickness (c,d). Scale bar: 50 µm. C) SEM characterization of the same SC and two zooms, indicated by the green and blue arrows (a), showing details of the top interface of SC (b) and an image of a tilted view showing the conformal adhesion of the SC to the patterned ITO substrate (c). Scale bars: 100 µm (a), 10 µm (b), 5 µm (c).

actual width of the evaporated gold line, we have carefully measured the active area using a confocal optical microscope in order to avoid uncertainty during the electrical characterization. Also, we considered the full width of the perovskite microwire, so that the active area was overestimated and therefore the extracted responsivity results to be conservative.

In Figure 1d, a picture of the final device with deposited gold contacts is shown. Optical image, at 10X magnification, of the final device is highlighted in the active region of the device. Furthermore, 3D confocal maps have been obtained in order to measure the thickness profile and the width of the microwires (Figure 1e). The thickness profiles (shown in Figure S1, Supporting Information) confirm the nominal thickness defined by the PDMS template, showing average values of 2.5 ± 0.34 µm and 6.2 ± 0.18 µm for nominal 2 µm-thick and 6 µm-thick microwires. The irregularities observed in Figure 1d might suggest the presence of short circuits. However, thickness profiles recorded across these features only reveal a reduction in perovskite thickness (see Figure S7, Supporting Information).

It can also be seen in the Figure 1 that the SC is in contact with the lateral ITO pads, leading to a parasitic lateral device. Measurements before and after gold metallization show, however, that this affects mostly dark current, while photoresponse is dominated by the vertical device due to the larger electric field (see Figure S6, Supporting Information).

## 2.2. Structural and Morphological Characterization

Final devices with a 6 µm-thick hybrid perovskite micro-wired single crystals, produced by microfluidic-assisted growth on patterned ITO (**Figure 2**A), were characterized by confocal and scanning electron microscopy (SEM), as reported in Figure 2B,C. The growth, macroscale self-assembly and 3D packing, driven by the microfluidic approach, are characterized directly on the real final device by confocal z-stack microscopy, in transmission mode and shown in Figure 2B. The Z-stack images (Figure 2B(a,c,d))

show homogeneous 3D crystalline microstructures, faithfully reproducing the microchannel used for confinement, without a significant presence of grain boundaries. The self-assembly growth technique does not alter the typical photoluminescence (PL) of MAPbBr$_3$, as shown by spatially resolved PL (SR-PL) spectra, directly acquired within the SC by confocal microscopy (Figure 2B(b)). The SEM image of the perovskite single-crystal shows that the deposition technique allows to obtain a single flat crystal with a regular shape, lateral dimensions exceeding hundreds of micrometers and a height comparable to the nominal 6 µm height of the microfluidic channel used for growth (Figure 2C). The images show a SC grown directly on the lower contact of the patterned ITO substrate. Zoom-in SEM images (Figure 2C(b,c)) clearly reveal smooth surfaces without visible voids and the angled facets without grain boundaries. Finally, crystal growth closely follows the pattern obtained on ITO by laser ablation.

Single crystal X-ray diffraction provides accurate measurements of individual diffraction effects, allowing to unequivocally assess the actual symmetry of the investigated phase.[25]

We assess the crystallographic quality of the microwire device core, looking for possible detectable distortions of the crystallographic unit cell due to the different synthesis conditions. Small single crystals, with a thickness of about 6 µm, were sampled starting from the microwires grown both at $T = 4$ °C and at room temperature (RT, $T = 24$ °C). The samples displayed well-formed smooth facets, with largest dimensions not exceeding 250 µm. Four distinct batches of the microwire material were examined, ensuring a reasonably complete sampling.

All the diffraction patterns were indicized with the expected cubic unit cell, typical of the Pm-3m most stable phase in standard ambient conditions. Some crystals show clear signs of twinning, despite their very small dimensions. A representative example of the recorded diffraction images can be seen in **Figure 3**, which displays the reconstructed projection of the diffraction pattern along the reciprocal axis b^*. The diffraction pattern confirms the symmetry of the lattice, apparent in the perfect square mesh of the reciprocal unit cell, and the high crystallographic quality
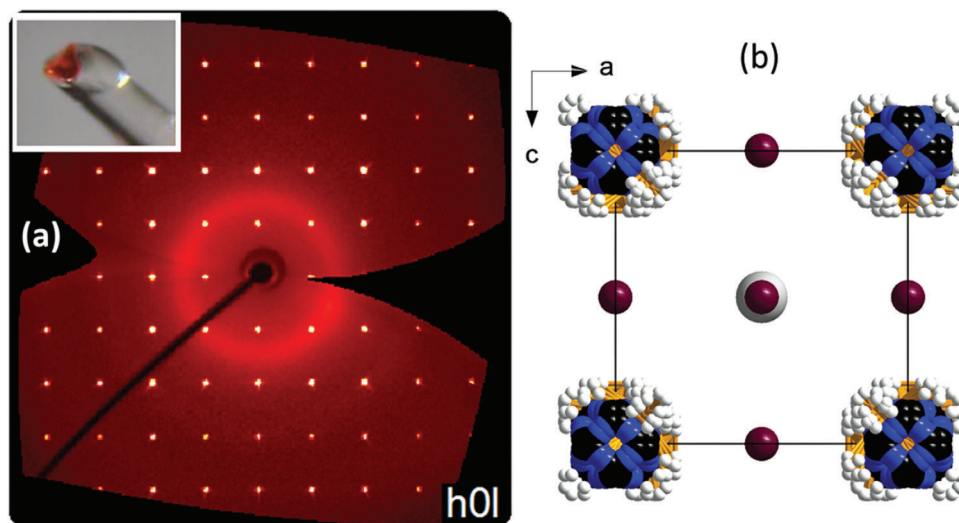
Figure 3. a) Reconstructed precession image of the diffraction output from the batch A sample. The reciprocal lattice equatorial plane h0l is shown. The square mesh of the cubic lattice down the reciprocal edge b* can be appreciated. The inset reports the probed crystal sample mounted on the top of a glass fiber with a drop of bi-component epoxy glue. The crystal dimensions are roughly 150 μm × 150 μm, with thickness of about 6 μm. b) Ball-and-stick atomic model of the unit cell of the perovskite at RT, as retrieved from the analysis of the diffraction pattern. Pb ions (gray) occupy the center of the cell and are octahedrally coordinated with Br (dark red). Methylamonium molecules are orientationally disordered at the corners (C: black; H: white; N: blue).

of the sample, which exploits minimal diffuse scattering effects and the absence of epitaxial twinning.

All the samples tested have average dimensions no greater than 0.11 mm. Our reference is a fragment cut from a thicker crystal, not directly connected with the microwire, which is a reasonable bulk control grown in the same conditions as the other ones. Full information on the examined crystals are available in Table S1, Supporting Information. All the experimental estimates for cell parameters lie within the range of measurements reported in literature for the same cubic phase ($a = 5.91950(10)$ Å,[26] $a = 5.9691(4)$ Å[27]), and are equal to the reference bulk sample within 3σ. The corresponding average cell edge length is $a = 5.927(2)$ Å.

From a crystallographic viewpoint, we conclude that the microwire material belongs to the expected cubic phase, with no appreciable differences among devices grown at low temperature or in ambient conditions.

2.3. Electrical Charaterization

Two devices with a thickness of 2 μm and 6 μm have been characterized under reverse bias. The area of the 2 μm and 6 μm thick devices are, respectively, 0.034 mm^2 and 0.013 mm^2. The JV curves for the 2 μm and 6 μm thick devices are shown in **Figure 4**a. The solid lines in the plot have been obtained under illumination with light at a wavelength of 500 nm with an equivalent incident photocurrent density of roughly 0.1 μA mm^{-2}. To obtain the current densities, we divided the measured currents by the nominal device area, extracted from optical microscopy images. The double-logarithmic plot of the current density (Figure S5, Supporting Information) shows the three characteristic regimes with slopes of 1, > 2 and 2, which are usually assigned to ohmic regime at low bias, trap-filled-limited (TFL) regime at intermedi-

ate bias, and space-charge limited current at higher voltages.[28] From the TFL region we can extract an approximate trap density in the order of $10^{14} - 5 \times 10^{14}$ cm^{-3}.

The measured incident photon to current efficiency (IPCE) for both devices results in values larger than 100% with reverse bias larger than 1.5 V, as shown in Figure 4b–d. This indicates the presence of gain in the two devices. The responsivity at a wavelength of 500 nm reaches in our devices roughly 100 AW^{-1}, with a photocurrent gain of about 200. The detectivity D^*, calculated from the responsivity $R(\lambda)$ and the dark current J_{dark} as $D^* = R(\lambda)/\sqrt{2qJ_{dark}}$, results in the range of $10^{12} - 10^{13}$ Jones, similar to what has been observed in ref. [29]. The responsivity and the detectivity of both devices are shown in Figures S2 and S3, Supporting Information.

The intensity of the monochromatic light source in the IPCE measurement was around 0.2 μW mm^{-2}, and the dark current has been corrected for by subtracting the measured current at wavelengths below the absorption edge. Both the JV curves and the observed photocurrent gain show similar behavior as reported in refs. [30,31] suggesting a similar mechanism at the origin of the gain. In particular, the qualitative similarity between the dark and light JV characteristics points to a photoresistive effect, possibly mediated by trap states. The linearity of the current response of the devices as function of the light intensity has been measured using a light-emitting diode (LED) source of 450 nm wavelength. For both devices, a reverse bias voltage of 2 V has been applied. The average current over six measurements and its uncertainty, calculated as the standard deviation of the average, is shown in **Figure 5**a, using the raw data reported in Figure S4, Supporting Information. The uncertainty on light intensity, resulting from the combination of the photodiode calibration and day-by-day variations, is estimated to give a relative contribution of 10%. A slightly super-linear behaviour is found within a light intensity variation of about a factor of eight. Based on the same
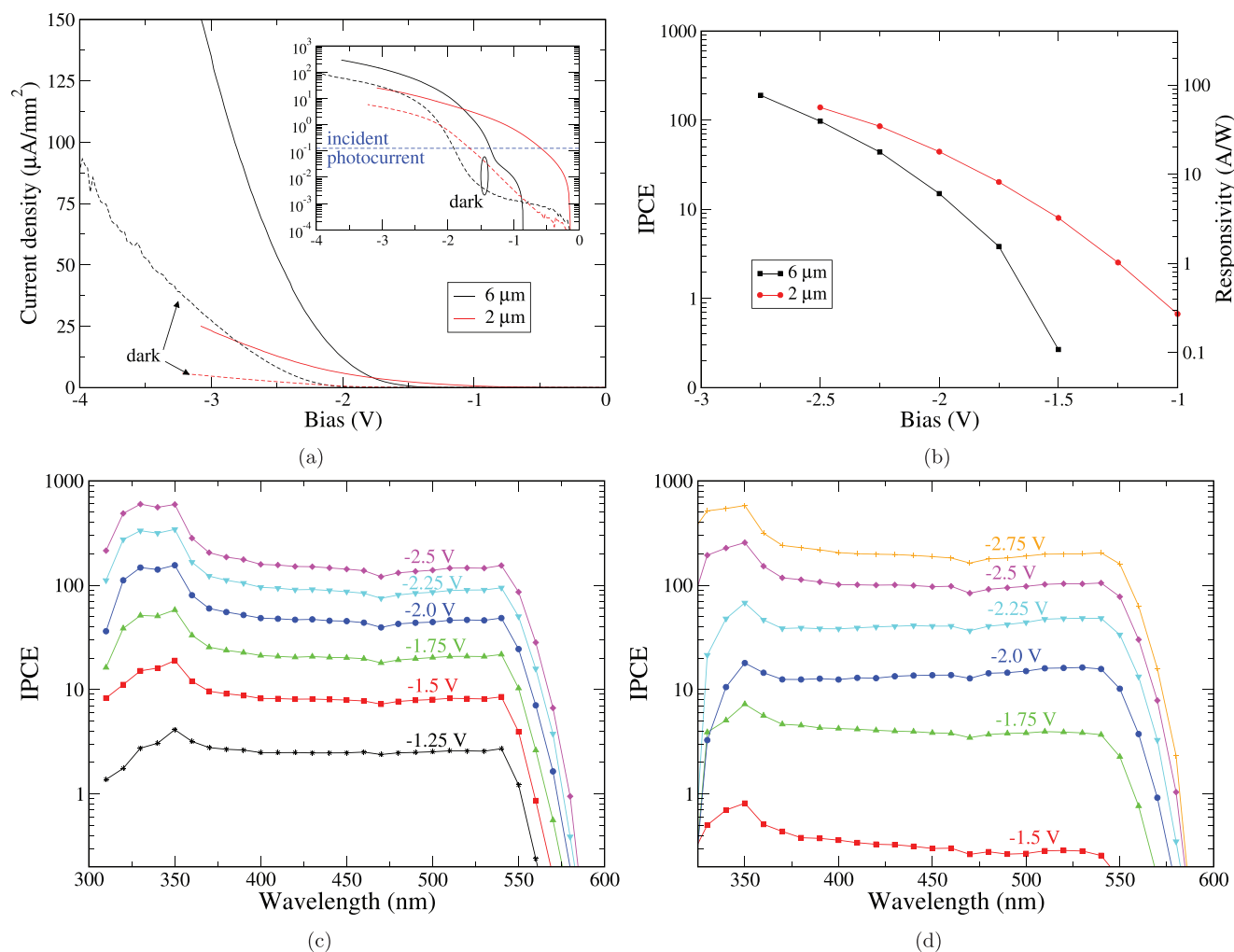
Figure 4. JV curve in dark and light conditions for the microchannels with 2 µm (red) and 6 µm (black) thickness (a). The dashed horizontal lines in the inset indicate the incident photocurrent. IPCE as a function of applied bias at $\lambda_0 = 500$ nm is shown in (b). IPCE as function of the wavelength at different bias voltages for the microchannels with 2 µm (c) and 6 µm (d) thickness. Data at wavelengths below 350 nm are not accurate due to absorption in the glass/ITO substrate.
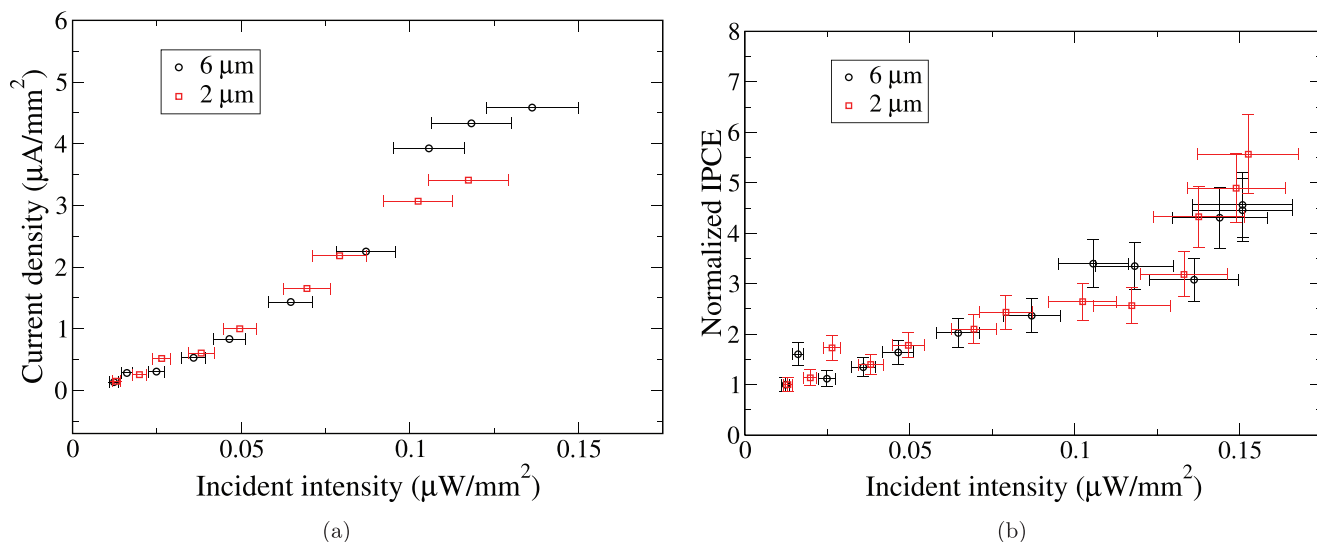
measurement data, the variation of the IPCE as a function of the light intensity is shown in Figure 5b. The IPCE values have been divided by the IPCE value at the lowest intensity. The increase as a function of the light intensity, similar to both devices, indicates that at least a component of the gain mechanism is related to a photoconductive effect. Also, the similar responses of both devices suggest that the difference in crystal thickness does not have an important effect on photocurrent gain.

To measure time response, the device has been connected to a preamplifier and a pulse shaper and the output voltage signal has been measured with an oscilloscope. The waveform of the response under a pulsed 450 nm wavelength LED of 0.16 µW mm^{-2} intensity is shown in **Figure 6**. To extract the rise time, which we defined as the time needed to reach the maximum of the signal, we have fitted the region around the peak by a double exponential function. The rise-time of the 6 µm (2 µm) thick device varies from 41.6 µs to 35.4 µs (45.6 µs to 26.8 µs) for applied voltages between −1.5 V and −3 V. This bias voltage variation corresponds to a gain variation of about a factor four. It is worthwhile

to note that the measured rise-times depend on the time constant given by the product of the resistance and capacitance (RC) of the sensor and of the electronics setup. While a decrease of the rise-time with the bias voltage could be expected due to a decrease of the sensor capacitance, a gain mechanism, like those related to trapping, may revert that behavior. This is not observed in the above measurements.

3. Conclusion

In summary, we have demonstrated the functionality of a photodetector based on MAPbBr$_3$ single crystals, obtained as microwires by a microfluidic-assisted growth directly on a patterned ITO substrate. The developed growth technique allows to obtain perovskite single crystals with high aspect ratios and positioned with extreme precision on specific regions of the device. Moreover, microfluidic-assisted growth allows to obtain SCs or network of crystals even on conductive patterns with different heights, thus paving the way for the effective realization

2300023 (6 of 9)

**ADVANCED
SCIENCE NEWS**

www.advancedsciencenews.com

**ADVANCED
MATERIALS
TECHNOLOGIES**

www.advmattechnol.de

Figure 5. a) Device current density as a function of incident light intensity from a blue LED with 450 nm wavelength. b) Normalized IPCE as a function of light intensity. The normalization is with respect to the IPCE at the lowest intensity to eliminate the dependency on the not exactly known device area. The measurement has been made at 2 V reverse bias. The error bars indicate the systematic uncertainty related to experimental setup as discussed in the text.
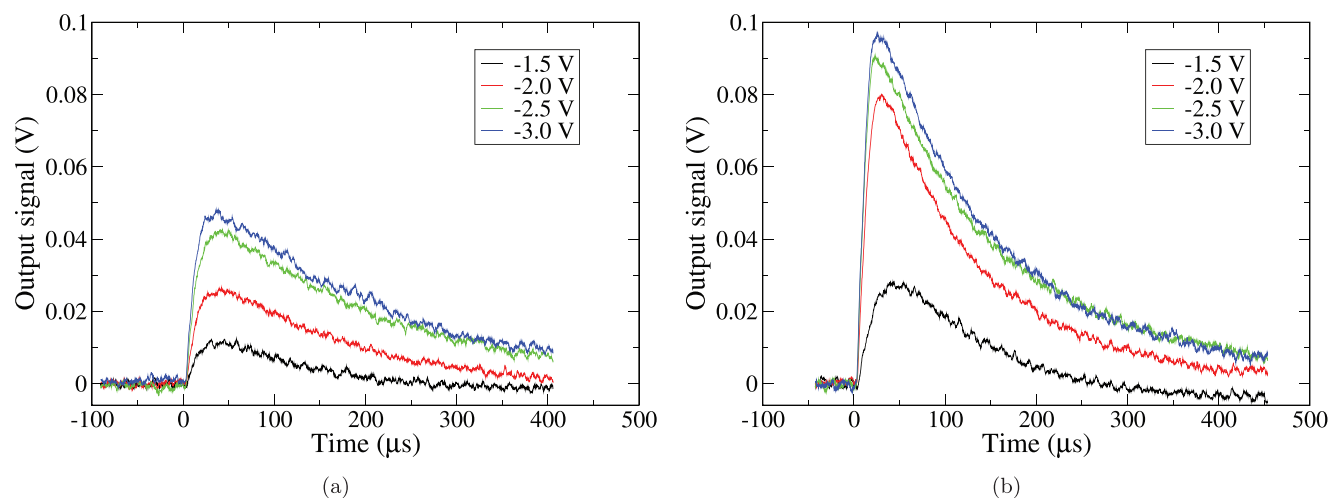
Figure 6. Waveform under pulsed LED illumination of 450 nm wavelength for the a) 6 μm and b) 2 μm thick devices.

of perovskite-based vertical photodetectors. The technique described in this paper also allows the extension to the fabrication of pixelated sensors over a large area. The photodetector shows gain increasing as a function of the bias, up to 200 at −2.5 V. The rise time is of the order of tens of μs, depending on the RC time constant of the electronic setup. The presence at the same time of a high responsivity and a short rise time makes the devices here described competitive with the state-of-art micro-sized photodetectors. All in all the results show that the microwires are promising candidates for the integration of perovskite with well-established silicon-based electronics.

4. Experimental Section

Lithography and Preparation of Microfluidic Template: Microfluidic-growth devices were fabricated using conventional soft lithography and replica molding technique from SU-8 (Microchem, YMC, Switzer-land) masters.[20] SU-8 masters were realized via standard optical lithography:[32] a thin layer of SU-8 negative photoresist was deposited onto a clean silicon substrate and the whole pattern of ad hoc designed photomasks (J.D. Phototools Ltd., Oldham, Lancashire, UK) was transferred on the photoresist film via UV exposure. The process has been optimized to obtain different heights of 2 ± 0.5 μm and 6 ± 0.5 μm for the microchannels.

Thereafter, the microfluidic-growth devices were obtained by replica molding, by casting a mixture of PDMS pre-polymer and curing agent (10:1, Sylgard-184, Dow Corning - USA) on the SU-8 master. The PDMS was then polymerized at 140 °C for 15 min and then detached from the master. To allow for the imbibition and the nucleation process of the perovskite, the microchannels were opened with a razor blade and the PDMS replica was placed in conformal contact and aligned on the patterned tracks on the glass/ITO substrate.

Microfluidic-Assisted Growth of Perovskite MicroWire Crystals: The perovskite MAPbBr$_3$ single crystals were grown by a microfluidic-assisted crystal growth method, as shown in Figure 1, using a precursor solution of methylammonium bromide and lead bromide (1:1) dissolved in DMF at a concentration in the range of 0.3–1.4 M. Different perovskite precursor

solutions with different molar concentrations were prepared in order to optimize the quality of single crystals. A small volume of precursor solution was dropped at one end of the PDMS microfluidic channel and was gradually imbibed into, filling up the microchannel under the effect of capillary forces. The device was left untouched at 4 °C for 18 h and then at 22 °C for 24 h. At the end of this process, the PDMS template was removed from the substrate leaving perovskite SCs on the conductive patterned ITO.

Using such a microfluidic-driven self-assembly approach several SCs growth experiments were carried on patterned ITO: SCs 2 µm-thick and 6 µm-thick with a width of 150 µm and a length greater than 600 µm were grown. All samples were prepared in an atmospheric environment. After the SC fabrication, a 80 nm-thick Au electrode has been deposited by thermal evaporation at ultra-high vacuum (9×10^{-6} mBar) using an evaporation rate equal to 0.3 Å s^{-1} for the first 10 nm and then increased up to 1 Å s^{-1}. Different SCs were characterized using confocal microscope (Olympus - FV1000 and Zeiss - LSM 980) and a field-emission scanning electron microscopy (FE-SEM, Auriga Zeiss). Incident photon-to-current efficiency (IPCE) spectra were acquired using a commercial setup (Arkeo-Adriadne, Cicci Research srl) based on a 300 W xenon lamp, able to acquire a spectrum from 300 nm to 1100 nm with a resolution of 2 nm.

XRD: Small single crystals, roughly 6 µm thick, were sampled from the multi-wire assemblies grown in different conditions with a stainless steel needle. The specimens were orange-colored, transparent, with largest dimensions not exceeding 150÷175 µm. All displayed well-formed smooth facets. The diffraction analysis was repeatedly carried out on various specimens cut from the microwire crystals to ensure a reasonable sampling of the whole batch. No differences were evident in either their unit cell or symmetry.

X-ray diffraction data were recorded at room temperature on a three-circle Bruker AXS Smart diffractometer equipped with a CCD area detector. Graphite-monochromated Mo Kα radiation ($\lambda = 0.71073$ Å) from a fine-focus sealed tube at a nominal source power of 50 kV × 30 mA was used throughout. Unit cell estimates came from the least squares fitting against the reciprocal lattice coordinates of a large number (>240) of accurately collected and integrated reflections. Possible systematic errors in the position of the instrumental zero were minimized by collecting reflections at both positive and negative 2θ. For each crystal, a hemisphere of the explorable space was scanned up to a maximum resolution of ≈ 1.10 Å, using a ω-scan strategy with $\Delta\omega = 0.2°$ or 0.3° and fixed sample-to-detector geometry ($2\theta = 0.0°$, $d = 50$ mm). The exposure time ranged from 20 to 40 s per frame, depending on the sample dimensions.

Laser Scanning Confocal Microscope: Laser scanning confocal microscope characterizations were performed by using a ZEISS LSM 980. A laser line at $\lambda = 405$ nm was used as an excitation source, equipped with a selective dichroic mirror, and 20X, 0.80 NA objective. All the images were obtained with resolution up to 1024 × 1024 pixels. The microscope was used in transmission mode by setting the pinhole aperture at 20–30 µm. Z-stack, 3D reconstruction, spatial analysis and spatially-resolved photoluminescence (PL) spectra were performed. The 3D confocal reconstruction was obtained by a Z-stack sequential acquisition and the optical sections have been collected in transverse *XZ* and *YZ* planes.

SEM Measurements: The surface morphology of the samples was characterized by scanning electron microscopy (SEM) using the Field-Emission Zeiss Auriga 405, equipped with a Quantax detector to collect electron diffraction X-rays (EDX) spectra. Instrument was equipped with a chamber room that maintained a pressure of about 10^{-5}–10^{-6} mbar. Micrographs were obtained at 1.5÷2 kV, with a backscattered detector and at varying working distance.

Linearity Measurements: A 450 nm wavelength LED had been used. The voltage bias was set and the current recorded by a KEITHLEY 2450 sourcemeter.

Time Measurements: A 450 nm wavelength LED with 1 ms width and a 1 Hz frequency had been used. The intensity of the light had been measured using a Thorlab FDS100-CAL calibrated photodiode. The data acquisition system was composed by a Cremat CR-111 charge sensitive preamplifier followed by Cremat CR-200-1 µs shaper. The output of the shaper was recorded using a standard oscilloscope.

Conflict of Interest

The authors declare no conflict of interest.

Data Availability Statement

The data that support the findings of this study are available from the corresponding author upon reasonable request.

[1] Z. Jiachen, J. Huang, *Adv. Sci.* **2017**, *5*, 1700256.

[2] Z. Yan, L. Chenglong, L. Shen, *InfoMat* **2019**, *1*, 164.

[3] H. Wei, J. Huang, *Nat. Commun.* **2019**, *10*, 1066.

[4] Y. Zhan, Q. Cheng, Y. Song, M. Li, *Adv. Funct. Mater.* **2022**, *32*, 2200385.

[5] G. Wang, D. Li, H.-C. Cheng, Y. Li, C.-Y. Chen, A. Yin, Z. Zhao, Z. Lin, H. Wu, Q. He, M. Ding, Y. Liu, Y. Huang, X. Duan, *Sci. Adv.* **2015**, *1*, 9.

[6] Y. Liu, F. Li, C. Perumal Veeramalai, W. Chen, T. Guo, C. Wu, T. W. Kim, *ACS Appl. Mater. Interfaces* **2017**, *9*, 11662.

[7] Y. Chen, J. Zhang, J. Zhou, Y. Chu, B. Zhou, X. Wu, J. Huang, *Adv. Opt. Mater.* **2018**, *6*, 1800469.

[8] Q. Ye, J. Zhang, P. Guo, H. Fan, D. Shchukin, B. Wei, H. Wang, *ACS Appl. Mater. Interfaces* **2018**, *10*, 43850.

[9] Z. Gu, Z. Zhou, Z. Huang, K. Wang, Z. Cai, X. Hu, L. Li, M. Li, Y. S. Zhao, Y. Song, *Adv. Mater.* **2020**, *32*, 1908006.

[10] C. Li, J. Li, C. Li, J. Wang, X. Tong, Z.-X. Zhang, Z. Yin, D. Wu, L. Luo, *Adv. Opt. Mater.* **2021**, *9*, 2100371.

[11] S. Wang, Z. Gu, R. Zhao, T. Zhang, Y. Lou, L. Guo, M. Su, L. Li, Y. Zhang, Y. Song, *Nano Res.* **2022**, *15*, 6568.

[12] B. Xin, Y. Pak, M. Shi, S. Mitra, X. Zheng, O. M. Bakr, I. S. Roqan, *Cell Rep. Phys. Sci.* **2021**, *2*, 100304.

[13] S. Li, Y.-S. Xu, C. Li, Q. Guo, G. Wang, H. Xia, H.-H. Fang, L. Shen, H.-B. Sun, *Adv. Mater.* **2020**, *32*, 2001998.

[14] L. Ren, G. Kunpeng, Q. tan, C. Qing, Q. wang, P. Yang, Y. Liu, *Appl. Opt.* **2021**, *60*, 8896.

ADVANCED
SCIENCE NEWS
www.advancedsciencenews.com

ADVANCED
MATERIALS
TECHNOLOGIES
www.advmattechnol.de

[15] W. Deng, X. Zhang, L. Huang, X. Xu, L. Wang, J. Wang, Q. Shang, S.-T. Lee, J. Jie, *Adv. Mater.* **2016**, *28*, 2201.

[16] W. Deng, J. Jie, X. Xu, Y. Xiao, B. Lu, X. Zhang, X. Zhang, *Adv. Mater.* **2020**, *32*, 1908340.

[17] S.-X. Li, H. Xia, X.-C. Sun, Y. An, H. Zhu, H.-B. Sun, *Adv. Funct. Mater.* **2022**, *32*, 2202277.

[18] Z. Chen, Q. Dong, Y. Liu, C. Bao, Y. Fang, Y. Lin, S. Tang, Q. Wang, X. Xiao, Y. Bai, Y. Deng, J. Huang, *Nat. Commun.* **2017**, *8*, 1890.

[19] W. Peng, L. Wang, B. Murali, K.-T. Ho, A. Bera, N. Cho, C.-F. Kang, V. Burlakov, J. Pan, L. Sinatra, C. Ma, W. Xu, D. Shi, E. Alarousu, A. Goriely, J.-H. He, O. Mohammed, T. Wu, O. Bakr, *Adv. Mater.* **2016**, *28*, 3383.

[20] Y. Xia, G. Whitesides, *Ann. Rev. Mater. Sci.* **1998**, *28*, 53.

[21] M. Cinquino, A. Fieramosca, R. Mastria, L. Polimeno, A. Moliterni, V. Olieric, N. Matsugaki, R. Panico, G. De Giorgi, M.and Gigli, C. Giannini, A. Rizzo, D. Sanvitto, L. De Marco, *Adv. Mater.* **2018**, *33*, 2102326.

[22] R. Iacobellis, S. Masi, A. Rizzo, R. Grisorio, M. Ambrico, S. Colella, P. F. Ambrico, G. P. Suranna, A. Listorti, L. De Marco, *ACS Appl. Energy Mater.* **2018**, *1*, 1069.

[23] I. Viola, F. Della Sala, M. Piacenza, L. Favaretto, M. Gazzano, M. Anni, G. Barbarella, R. Cingolani, G. Gigli, *Adv. Mater.* **2007**, *19*, 1597.

[24] N. Ghofraniha, I. Viola, F. Di Maria, G. Barbarella, G. Gigli, C. Conti, *Laser Photonics Rev.* **2013**, *7*, 432.

[25] L. Lo Presti, J. Parravicini, R. soave, G. Parravicini, M. Mauri, L. Loconte, F. Di Mei, F. Falsi, L. Tartara, S. Binetti, J. A. Aharon, E. DelRe, *Phys. Rev. B* **2020**, *102*, 214110.

[26] G. A. Elbaz, D. B. Straus, O. E. Semonin, T. D. Hull, D. W. Paley, P. Kim, J. S. Owen, C. R. Kagan, X. Roy, *Nano Lett.* **2017**, *17*, 1727.

[27] Y. Wang, X. Lü, W. Yang, T. Wen, L. Yang, X. Ren, L. Wang, Z. Lin, Y. Zhao, *J. Am. Chem. Soc.* **2015**, *137*, 11144.

[28] V. M. Le Corre, E. A. Duijnstee, O. El Tambouli, J. M. Ball, H. J. Snaith, J. Lim, L. J. A. Koster, *ACS Energy Lett.* **2021**, *6*, 1087.

[29] C. H. Ji, K. T. Kim, S. Y. Oh, *RSC Adv.* **2018**, *8*, 8302.

[30] K. Domanski, W. Tress, T. Moehl, M. Saliba, M. K. Nazeeruddin, M. Grätzel, *Adv. Funct. Mater.* **2015**, *25*, 6936.

[31] R. Dong, Y. Fang, J. Chae, J. Dai, Z. Xiao, Q. Dong, Y. Yuan, A. Centrone, X. C. Zeng, J. Huang, *Adv. Mater.* **2015**, *27*, 1912.

[32] A. Zizzari, V. Arima, A. Zacheo, G. Pascali, P. Salvadori, E. Perrone, D. Mangiullo, R. Rinaldi, *Microelectron. Eng.* **2011**, *88*, 1664.